High-Resolution Resistless Nanopatterning on Polymer and Flexible Substrates for Plasmonic Biosensing Using Stencil Masks

Oscar Vazquez-Mena,[†,*] Takumi Sannomiya,[‡] Mahmut Tosun,[†] Luis G. Villanueva,[†] Veronica Savu,[†] Janos Voros,[‡] and Juergen Brugger[†,*]

[†]Microsystems Laboratory, Ecole Polytechnique Fédérale de Lausanne (EPFL), 1015 Lausanne, Switzerland and [‡]Laboratory of Biosensors and Bioelectronics, Eidgenössische Technische Hochschule Zürich (ETHZ), 8092 Zurich, Switzerland

ABSTRACT

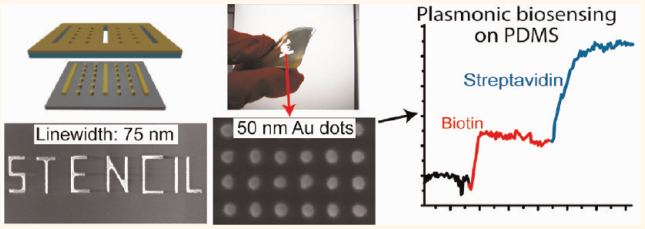

The development of nanoscale lithographic methods on polymer materials is a key requirement to improve the spatial resolution and performance of flexible devices. Here, we report the fabrication of metallic nanostructures down to 20 and 50 nm in size on polymer materials such as polyimide, parylene, SU-8, and PDMS substrates without any resist processing using stencil lithography. Metallic nanodot array analysis of their localized surface plasmon spectra is included. We demonstrate plasmon resonance detection of biotin and streptavidin using a PDMS flexible film with gold nanodots. We also demonstrate the fabrication of metallic nanowires on polyimide substrates with their electrical characteristics showing an ohmic behavior. These results demonstrate high-resolution nanopatterning and device nanofabrication capability of stencil lithography on polymer and flexible substrates.

KEYWORDS: stencil · nanodots · nanowires · biosensors · plasmonic · flexible substrates · nanopatterning

The development of advanced and complex devices on polymer substrates such as flexible electronics[1−3] and sensors,[4] artificial skins[5] and muscles,[6] biomedical devices, polymer memory devices,[7] and flexible solar cells[8] has brought a wide range of novel applications due to their flexibility and adaptability to nonplanar surfaces. The performance of such devices can be significantly improved by fabricating and integrating nanostructures on polymer substrates, increasing their feature density and introducing novel functionalities. However, a major limitation is that conventional nanofabrication is based on rigid silicon technology and chemical resist processing that normally is not suitable for flexible polymer materials. Recently, considerable advances in resistless nanopatterning have been reported based on transferring prefabricated nanostructures to diverse substrates using multistep fabrication processes. High-quality nanostructures have been printed with high order and density using directed assembly,[9] transfer printing,[10,11] microdroplet molding,[12] and liquid-bridge-mediated nanotransfer molding.[13] Using a much simpler approach, herein we describe a complementary alternative using direct patterning by stencil lithography (SL) to fabricate metallic nanostructures on polymers.

Stencil lithography is a novel technique based on parallel shadow mask patterning for metal deposition, as illustrated in Figure 1a.[14] SL is also very versatile and has been used for patterning with dry etching and ion implantation processes, as well.[15,16] A major advantage of SL is that stencil masks can be reused several times for cost-efficient nanofabrication.[17−19] SL also has broad material compatibility because no resist processing, chemical solvents, energy radiation, or mechanical pressure are involved, allowing nanofabrication on diverse materials like polymers that are typically less resistant to such treatments. This is of great benefit compared to conventional nanofabrication techniques like electron-beam lithography (EBL) or deep-UV and nanoimprint lithography based on chemistry resist processing. In fact, micrometer-scale organic transistors and metallic wires have successfully been fabricated by SL on polymer

* Address correspondence to juergen.brugger@epfl.ch, ovazquez@berkeley.edu.

Received for review March 27, 2012 and accepted May 17, 2012.

Published online May 17, 2012
10.1021/nn301358n

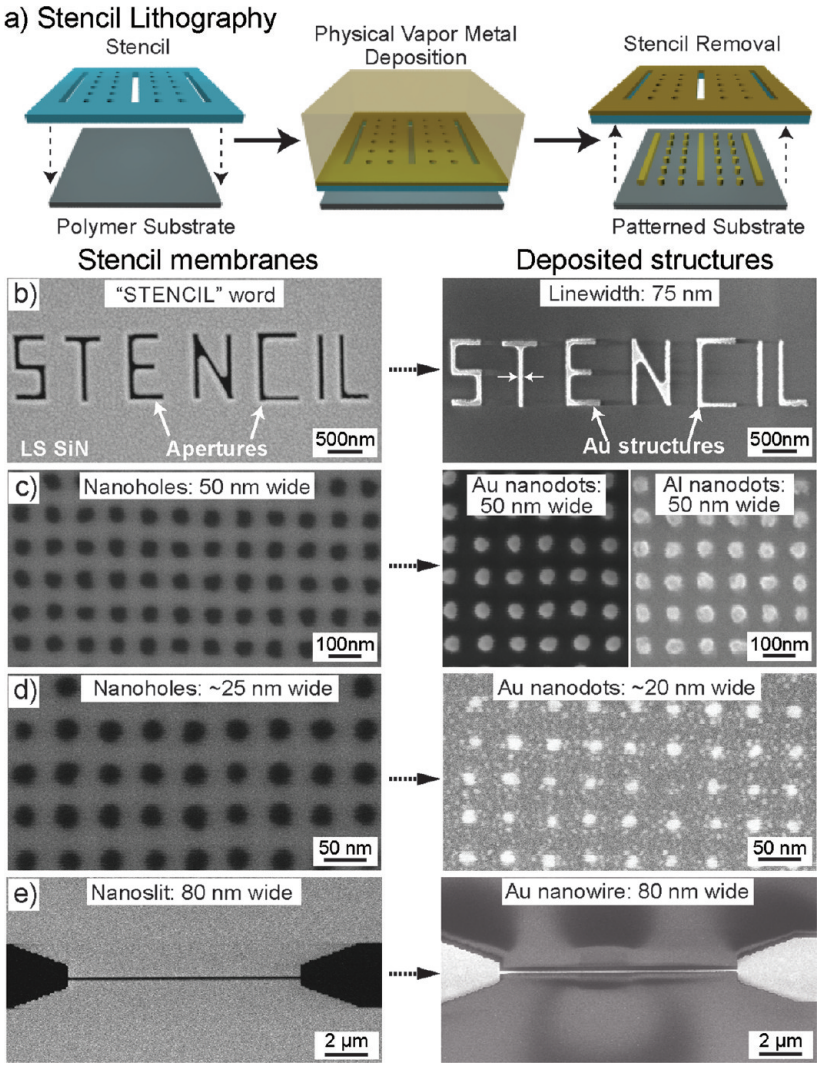

Figure 1. Stencil lithography on polymer substrates. (a) Schematic illustration of resistless and parallel patterning by stencil lithography. First, a stencil is put on top of a substrate followed by the vapor deposition of metal through the stencil apertures, reproducing the patterns onto the substrate. Finally, the stencil is removed from the substrate. (b–e) SEM images of LS SiN stencil membranes with nanoapertures (left column) and their corresponding deposited structures (right column) showing the stencil-to-substrate pattern transfer. (b) Word "STENCIL" made of Au with 75 nm line width deposited on SU-8. (c) Arrays of high-resolution 50 nm wide Au and Al nanodots deposited on polyimide. (d) Array of 20 nm wide Au nanodots deposited on SU-8. (e) A 10 μm long and 80 nm wide Au nanowire between two side micrometric pads deposited on polyimide.

flexible substrates.[20,21] Nanoscale patterning on polymer substrates has also been demonstrated for nanodots[22] and nanoantennas.[23] The results presented in this work demonstrate a major improvement in resolution down to ~50 and ~20 nm, realizing metallic nanodots and nanowires and demonstrating a biosensor on a flexible PDMS substrate. Herein we present high-quality gold and aluminum nanodots down to 50 nm in size with 50 nm half-pitch fabricated on four relevant polymer substrates: polyimide (PI), epoxy (SU-8), parylene (PL), and polydimethylsiloxane (PDMS). We analyze the plasmon spectra of the Au nanodots deposited on the polymers, showing high-quality resonance peaks and the effect of radiative coupling. Similarly, we present Au nanowires on polyimide with their corresponding electrical characteristics. We also demonstrate biosensing on flexible substrates based on localized surface plasmon resonance using Au nanodots deposited on PDMS, showing the capability of stencil lithography to realize devices on flexible substrates.

RESULTS AND DISCUSSION

The stencils for this study consisted of 100 nm thick low-stress silicon nitride (LS SiN) membranes patterned by EBL and etching, supported by 6 × 6 mm^2 and 2 × 2 cm^2 size silicon chips, for nanodots and nanowire depositions, respectively. PI, SU-8, and parylene polymer substrates consisted of 2 μm thick films deposited on glass or silicon wafers. For nomenclature, these samples are labeled as "PI/Si" for PI on silicon or "SU-8/glass" for SU-8 on glass. The PDMS substrates

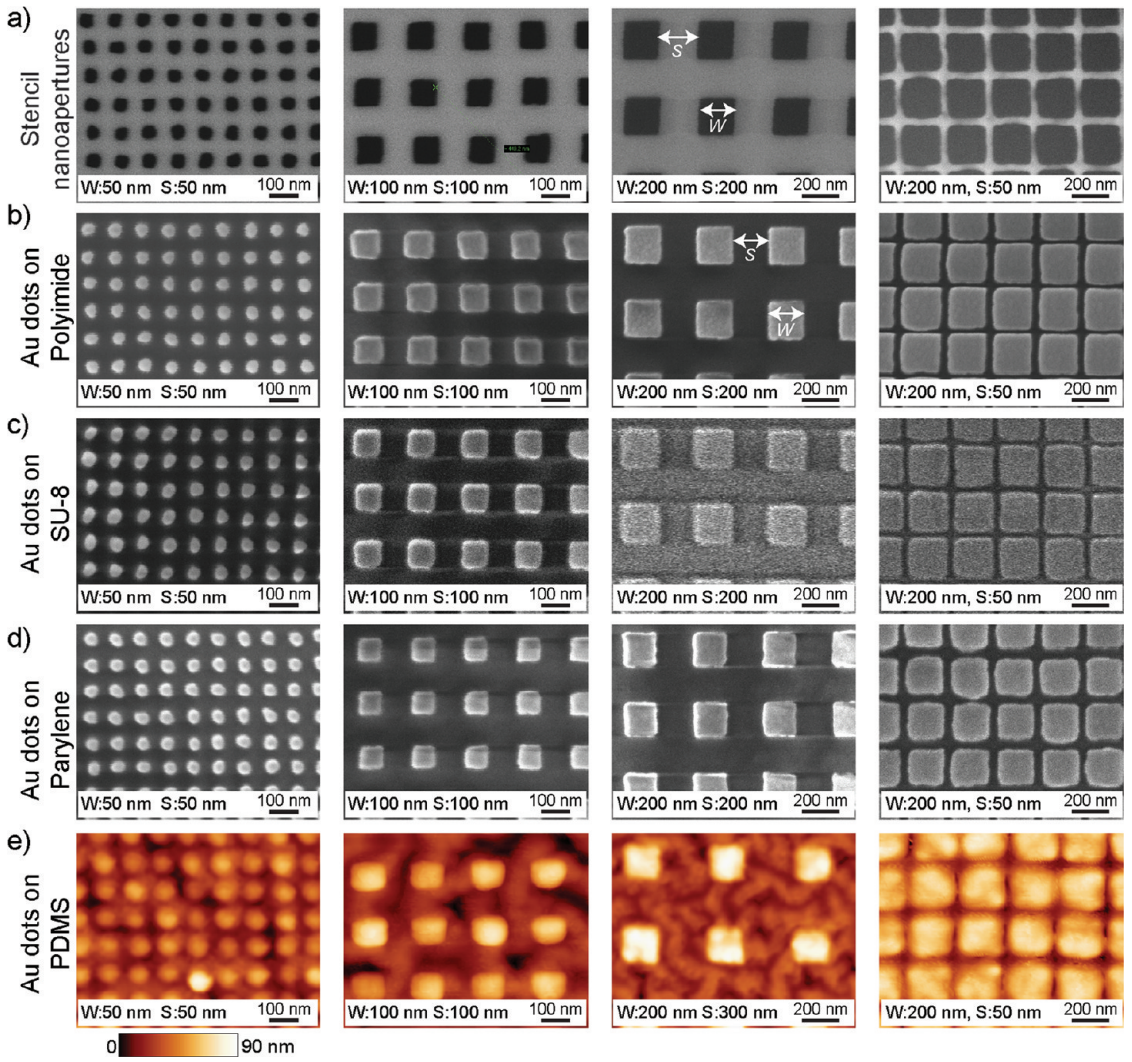

Figure 2. Au nanodots on polymer substrates by stencil lithography. (a) SEM images of stencil membranes with different nanohole size (*W*) and interdot spacing (*S*) of *W* = 50 nm and *S* = 50 nm, *W* = 100 nm and *S* = 100 nm, *W* = 200 nm and *S* = 200 nm, and *W* = 200 nm and *S* = 50 nm. (b–d) SEM micrographs of the Au nanodots deposited through the corresponding stencils on polyimide, SU-8, and parylene films on silicon wafers. (e) AFM topography images of Au nanodots deposited on PDMS. The deposited nanodots reproduce the stencil aperture patterns forming high-resolution nanostructures on the polymer substrates. Optical pictures of the nanohole and nanodot arrays and of the PDMS patterned flexible substrates are shown in the Supporting Information-1. SEM images of the complete sets of Au and Al nanodot arrays with different sizes and spacing are shown in the supporting images.

were free-standing 2 mm thick flexible films. To deposit the metallic nanostructures, the stencils were fixed on the substrates with metallic adhesive tape followed by physical vapor metal deposition. In the case of Au nanostructures, a 45 nm thick Au layer was deposited at 1 Å/s deposition rate by electron-beam evaporation with a 5 nm thick Ti (4 Å/s) adhesion layer. For Al nanostructures, a 30 nm thick layer was deposited at 1 Å/s also by electron-beam evaporation. The depositions were done at room temperature and 10^{-6} mbar pressure using a Leybold LAB-600 electron-beam evaporator. The distance from the material source to the substrate is 1 m, and the source of material has a diameter of 5 mm. The stencils, the patterned substrates, and the flexible PDMS films are shown in the Supporting Information-1. The stencil fabrication process and sample preparation are shown in the Supporting Information-2.

The capability of SL for patterning high-resolution metallic nanostructures is demonstrated in Figure 1b–e, showing stencil nanoapertures with their corresponding deposited nanostructures on polymer substrates: (b) the word "STENCIL" with ~75 nm line width made of Au and deposited on SU-8/Si, (c) Au and Al nanodots 50 nm wide on PI/Si, (d) Au nanodots 20 nm wide on SU-8/Si, and (e) a Au nanowire 80 nm wide on PI/Si. To determine the resolution power of stenciling on polymers, we prepared stencils with nanohole arrays with systematic variation of width and interhole spacing. The arrays were 30 × 30 μm^2 in size with nanohole width (*W*) from 50 to 200 nm and interdot edge-to-edge spacing (*S*) from 50 to 300 nm. Figure 2 shows

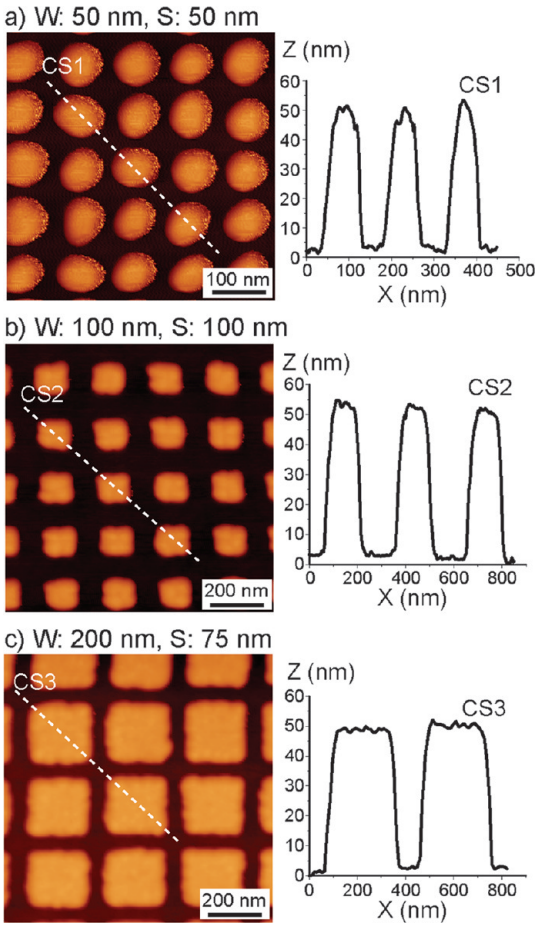

Figure 3. AFM analysis of Au nanodots on polymer substrates (SU-8). AFM images and line profiles of Au nanodots deposited on a SU-8/glass substrate for different nanodot arrays: (a) $W = 50$ nm, $S = 50$ nm; (b) $W = 100$ nm, $S = 100$ nm; and (c) $W = 200$ nm, $S = 75$ nm. The images and profiles show that the dots have the expected nominal thickness of 50 nm and the absence of scattered material between the dots. AFM images of nanodot arrays on the other polymers are shown in the supporting images.

representative results of the stencil apertures with their corresponding deposited Au nanodots, demonstrating fabrication of high-density 50−200 nm wide nanodots with spacing down to 50 nm. The nanodots have very high structural quality, showing high-resolution nanopatterning on polymers by SL. Figure 3 shows AFM topography images and line profiles of Au nanodots deposited on SU-8/glass, confirming the high resolution of the nanodots. AFM also shows that the thickness of the structures corresponds to the nominal value of 50 nm. Similarly, Al nanodots were patterned on SU-8/Si substrates achieving also high resolution down to 50 nm, as observed in Figure 1c. Images of Al nanodots 50−200 nm wide are shown in Supporting Information-3. Smaller Au nanodots 20 nm wide were realized on SU-8/Si, as shown in Figure 1d. However, their resolution and quality was limited by the blurring phenomenon and the clogging of the nanoapertures, indicating the resolution limits of the technique for the used configuration. AFM data of the ∼20 nm Au nanodots are shown in the Supporting Information-4.

A well-known effect in SL is blurring, which is the enlargement of the deposited structures with respect to the stencil apertures.[19,24−26] The blurring is due to a combined effect of two factors: (i) the spatial gap between the stencil and the substrate and (ii) the surface diffusion of the deposited atoms (Supporting Information-5). Previous works on stenciled Au nanostructures on silicon and glass substrates have shown the presence of scattered particles around the deposited structures and a thickness reduction of the structures due to blurring.[27] SEM and AFM analyses in Figure 2 and Figure 3 clearly indicate that blurring is strongly reduced for depositions on polymer substrates compared to bare glass or silicon substrate depositions reported previously,[27] thus improving significantly the quality of the nanostructures (Supporting Information-6). We attribute this to a smaller stencil−substrate gap (<1 μm), due to a better contact of silicon nitride stencils with polymer substrates compared to the case using glass or silicon substrates. This is probably associated with the flexibility, softness, and adhesion forces of the polymers related to electrostatic charges and van der Waals forces,[28] resulting in larger contact areas and a smaller stencil−substrate gap. Similarly, interactions between polymer molecules and the deposited atoms play a significant role in the surface diffusion and can also reduce the blurring.[19]

An important property of metallic nanodots is the electromagnetic field enhancement due to localized surface plasmon resonance (LSPR).[29] Integrating plasmonic structures on polymer substrates can bring significant improvements for flexible sensing and photonic and optoelectronic devices. Hence, we measured the extinction spectra of Au nanodots on the polymer substrates. The spectra have well-defined LSPR peaks within the visible-IR range, as shown in Figure 4a,b for W = 50 and 200 nm Au nanodots with varying spacing. The complete LSPR spectra for all widths and spacing are shown in Supporting Information-7. The resonance wavelength (λ_R) depends on the nanodot size and spacing, as shown in Figure 4c. The Au nanodots on all four polymers show similar trends with variations due to their different refractive indexes. In fact, the 200 nm wide nanodots on PDMS, which has the lowest refractive index, show the smallest red shift (λ_R increase) with spacing as expected. The largest nanodots (W = 150 and 200 nm) show a significant red shift as the spacing increases attributed to far-field interactions between nanodots (radiative coupling), proportional to the polarizability and size of the nanodots.[30] Similar spacing-related red shifts are reported for nanodots on rigid glass substrates made by resist-based nanofabrication methods[30,31] and by SL.[27] For the smaller nanodots of W = 50−100 nm, the far-field interaction is not observed. It is worth noting that

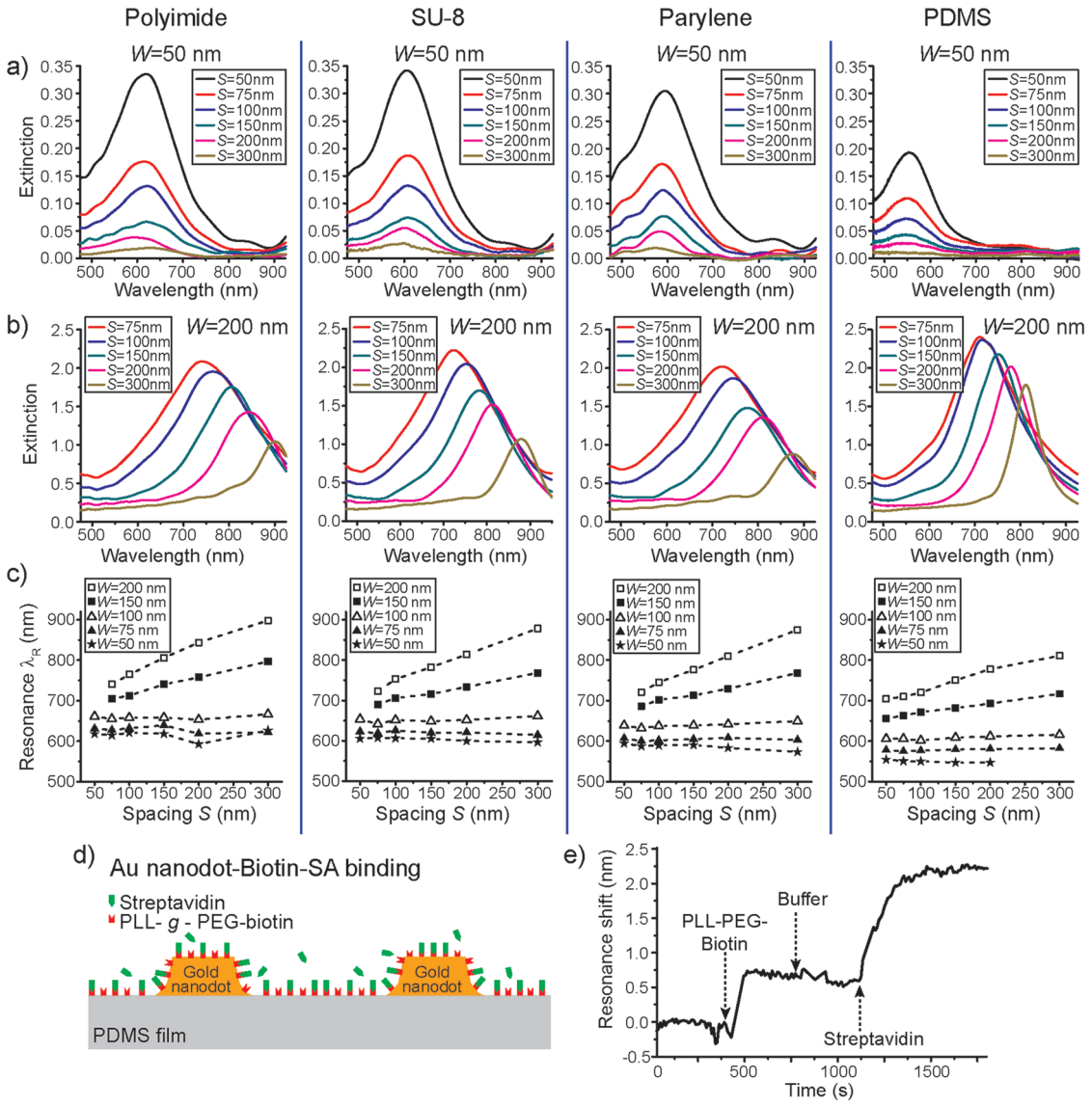

Figure 4. LSPR and biosensing with Au nanodot arrays on polymers. Extinction spectra for (a) $W = 50$ nm and (b) $W = 200$ nm nanodots with varying spacing S, showing LSPR peaks on all four polymer substrates. (Refractive indexes: (PI) $n = 1.7$, (SU-8) $n = 1.67$, (PL) $n = 1.64$, (PDMS) $n = 1.4$.) (c) Plots of λ_R as function of spacing (S) and size (W) showing a λ_R red shift as the spacing increases for $W = 200$ and 150 nm nanodots. For the smaller nanodots, $W = 50-100$ nm, there is no clear change in λ_R with spacing. All extinction spectra are shown in Supporting Information-7. (d) Schematics of biosensing experiments with nanodots on PDMS. Au nanodots and PDMS are biotin-functionalized, and then streptavidin binds to biotin. (e) LSPR shift of an array of $W = 75$ nm and $S = 50$ nm Au nanodots on PDMS upon the addition of biotinylated molecules and streptavidin. The arrows indicate the addition of biomolecules and buffer rinsing.

near-field interactions (static-dipole coupling) are not observed in the extinction spectra of the stenciled nanodots. This coupling manifests as a blue shift (λ_R decrease) when the spacing increases in the $S < 50$ nm range.[32,33] The absence of near-field interactions is also a strong indication of a strongly reduced blurring; otherwise, shortening of the spacing and scattered particles between the nanodots would produce a blue shift due to near-field coupling as observed for the case of nanodots on silicon oxide substrates[27] (Supporting Information-6).

The potential of SL to fabricate nanoscale devices on polymer substrates is demonstrated implementing a LSPR-based biosensor on a PDMS substrate. An array of Au nanodots, $W = 75$ nm and $S = 50$ nm, was used for detecting biotin and streptavidin (SA) based on LSPR wavelength shift upon biomolecule adsorption.[34−36] The nanodots are functionalized with biotin to which SA binds selectively, as schematically illustrated in Figure 4d. The concentration of the SA solution is 370 nM. The resonance shift ($\Delta\lambda_R$) time response is plotted in Figure 4e. The measurement starts with a HEPES pH 7.4 buffer solution to obtain a baseline. When biotin (PLL-*g*-PEG-biotin) is injected and adsorbed on the Au nanodots, a first resonance shift of $\Delta\lambda_R \sim 0.7$ nm is observed. Then, after SA is injected, an additional $\Delta\lambda_R$ of ~1.7 nm is produced. The resonance shift is larger

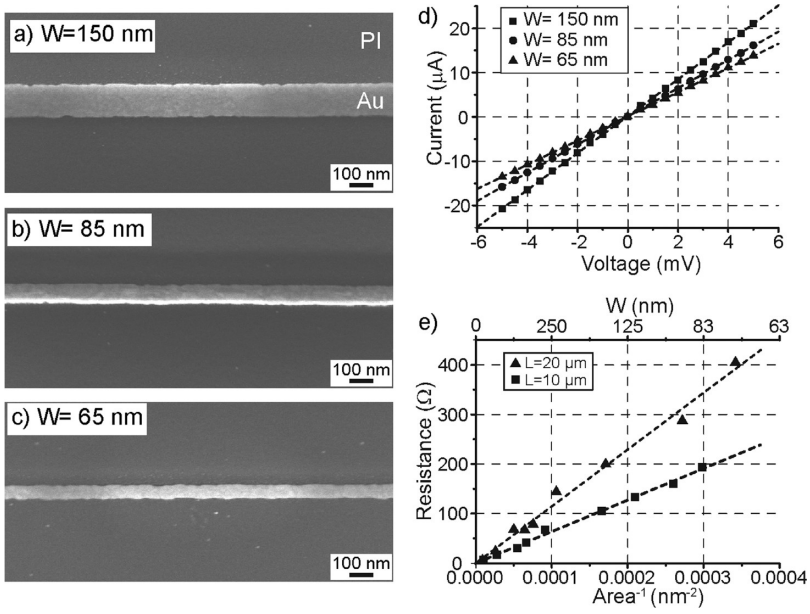

Figure 5. Au nanowires on Pl substrate. (a−c) Au nanowires deposited on a Pl/silicon substrate with widths of 150, 85, and 65 nm, respectively, and 20 μm long. The nanowires have a thickness of 40 nm. (d) *I*/*V* characteristics at room temperature of the nanowires show a linear response as expected for ohmic metallic structures. (e) Resistance of the nanowires as a function of the inverse cross section area A^{-1}. The width is extracted from SEM images and the thickness from AFM measurements. The contact resistance contribution has been subtracted for the plot. The dashed lines indicate linear fittings. Details on the electrical characterization are given in Supporting Information-9.

than the noise level, clearly showing binding events. Even though this resonance shift is smaller than previous reports for similar experiments,[27,34] the results demonstrate the capability of stencil lithography to realize biosensing devices on a flexible substrate using stencil deposition of nanostructures on a PDMS film. Experimental details and PLL-*g*-PEG-biotin are shown in Supporting Information-8.

Nanowires are also central for implementing nanoelectronic devices on polymer substrates. Using stencils with nanoslits, we fabricated Au/Ti nanowires 10 and 20 μm long, 40 nm thick, on Pl/silicon substrates as shown in Figure 1e. Figure 5a−c shows Au nanowires 150, 85, and 65 nm wide (20 μm long). Au/Ti electrical contacts were deposited on the nanowires using a second stencil deposition. The linear *I*−*V* curves of the Au nanowires measured at room temperature shown in Figure 5d indicate an ohmic behavior as expected for metallic nanowires. The resistance as a function of the inverse cross section area (A^{-1}) is plotted in Figure 5e, allowing the extraction of a resistivity of $\rho = 6.05\ \mu\Omega$cm. This resistivity is larger than Au bulk resistivity of 2.2 $\mu\Omega$cm at room temperature. This increment is expected for metallic nanostructures with dimensions comparable to the electron mean free path (~40 nm for Au at 300 K) as in our case.[37] The measured resistivity is in accordance with previous reports of Au nanowires on silicon oxide fabricated by e-beam lithography[38] and by SL ($\rho = 5.16\ \mu\Omega$cm).[39] (Nanowire contacting and resisitivity analyses are shown in Supporting Information-9.)

CONCLUSIONS

In conclusion, we have demonstrated a simple, straightforward, and scalable resistless parallel fabrication of high-resolution and high-density nanostructures down to 50 nm on a variety of relevant polymer substrates. The extinction spectra of the nanodots show LSPR in the visible-IR range suitable for plasmonic applications. The application of the nanodots for biosensing demonstrates the potential of this technique to realize plasmonic devices on polymer and flexible substrates. Similarly, the metallic nanowires with ohmic behavior can be used for interconnections on polymer materials. These results also prove that stencil lithography is a promising and ready technique to integrate nanotechnology developments on soft flexible and polymer-based devices. Further work shall concentrate to better understand and reduce blurring, increase the patterning area to large scale, and demonstrate high-resolution patterning on other polymer materials.

METHODS

Stencil Fabrication. The stencils were fabricated using 100 mm diameter ⟨100⟩ silicon wafers. First, a 100 nm thick LS SiN layer is deposited by low-pressure chemical vapor deposition. Then, nanoapertures in the LS SiN are patterned by e-beam lithography and dry etching. Conventional UV lithography on the backside

of the wafer is used to form windows to release the patterned membranes. The bulk silicon is etched by deep reactive ion etching followed by KOH wet etching. After membrane release, the wafers are cleaved into chips. In the case of stencils for nanodots, the nanoholes have widths (W) of 50−75−100−150−200 nm and interdot edge-to-edge spacing (S) of 50−75−100−150−200−300 for each width. The stencil fabrication process is explained in detail in the Supporting Information-7.

Substrate Preparation. Polyimide (PI-2610, HD Microsystems) was spin coated on silicon and glass wafers followed by a curing process. SU-8 (GM1040, Gersteltec) was also spin coated on silicon and glass wafers, followed by a UV exposure and baking. Parylene-C was deposited by chemical vapor deposition on silicon and glass wafers. PDMS (Sylgard 184, Dow Corning, USA) was prepared by mixing the base polymer and curing agent with 10:1 ratio. The mixture was degassed, poured into a Petri dish and cured. The detailed preparation of the substrates is given in Supporting Information-7.

Deposition Conditions. In the case of Au nanostructures, a Ti adhesion layer 5 nm thick followed by Au 45 nm thick was deposited through the stencils by electron-beam physical vapor deposition. Au was deposited at a rate of 1 Å/s and Ti at 4 Å/s. In the case of Al nanostructures, a 30 nm thick layer was deposited at 1 Å/s. The depositions were done at room temperature and at 10^{-6} mbar pressure using a Leybold LAB-600 evaporator. The distance from the material source to the substrate is 1 m, and the source of material has a diameter of 5 mm.

Extinction Spectra Measurements. The extinction spectra of the nanodots were measured on the transparent substrates: PI/glass, SU-8/glass, PL/glass, and PDMS. The spectra were measured in the 450−950 nm range. The spectra were acquired with a spectrophotometer SpectraPro 2150, Pixis 400, Princeton Instruments (U.S.A.) equipped with an optical microscope, Axiovet 200, Carl Zeiss (Germany). A halogen lamp with parallel illumination was used. The characteristic oscillation spectral features due to the interference within the 2 μm thick polymer layer (polyimide, SU-8, and parylene) were removed by Fourier filtering in $1/\lambda$ space. A parabolic function was used to detect the resonance wavelength.

Biosensing Measurements. Biosensing measurements were done using 75 nm wide nanodots with 50 nm spacing on a PDMS film. The measurements were carried in 160 mM salt buffer solution adjusted to pH 7.4 containing 10 mM of 4-(2-hydroxyethyl)piperazine-1-ethanesulfonic acid (HEPES) with 150 mM NaCl. The Au nanodots were functionalized with a biotinylated poly(L-lysine)-*g*-poly(ethylene glycol), PLL-*g*-PEG-biotin. The concentration of the PLL-*g*-PEG-biotin solution was 100 μg/mL. The streptavidin (SA) solution had a concentration of 20 μg/mL. The measurements were done with a flow cell containing the PDMS film with the nanodot arrays. The area of the sensing measurements was 30 × 1.5 μm^2. The PLL-*g*-PEG-biotin molecule is shown in the Supporting Information-8.

Electrical Characterization of Nanowires. A second stencil containing micrometric apertures (~300 μm) was used to deposit electrical contacts on the nanowires. The *I*/*V* curves were measured using a probe station in two-probe configuration at room temperature in DC mode. The *I*/*V* data were used to obtain the resistance of the devices (R_M), which includes the resistance of the nanowires (R_{NW}) and the contact resistance (R_C). The area cross section of the wires was obtained from their width measured with SEM and from their 40 nm thickness. The contact resistance (R_C) and resistivity (ρ) of the nanowires were obtained by linear fitting the data set of R_M *versus* A^{-1} to the expression

$$R_M = R_C + R_{NW} = R_C + \rho_{NW}\frac{L}{A}$$

From the linear fitting, R_C and ρ can be independently extracted since the length L of the nanowires is known. The value of R_C can be subtracted from R_M to obtain R_{NW}, which is plotted in Figure 5e. The electrical contacting of the nanowires and the resistivity analysis are described with more details in Supporting Information-9.

Conflict of Interest: The authors declare no competing financial interest.

Supporting Information Available: The supporting images file contains images of the complete set of stencil membranes with their corresponding nanodot arrays. The other file contains optical images of nanodot arrays and PDMS substrate, stencil fabrication, and substrate preparation, images of aluminum nanodots, images of 20 nm wide gold nanodots, gap and blurring discussion, comparison of stencil depositions on oxide and polymer substrates, extinction spectra of full set of nanodots, description of biosensing measurements and PLL-*g*-PEG-biotin molecule, and a description of the electrical analysis of nanowires. This material is available free of charge *via* the Internet at http://pubs.acs.org.

REFERENCES AND NOTES

1. Ko, H. C.; Stoykovich, M. P.; Song, J.; Malyarchuk, V.; Choi, W. M.; Yu, C.-J.; Geddes, J. B., III; Xiao, J.; Wang, S.; Huang, Y.; *et al.* A Hemispherical Electronic Eye Camera Based on Compressible Silicon Optoelectronics. *Nature* **2008**, *454*, 748–753.
2. Lacour, S. P.; Jones, J.; Wagner, S.; Li, T.; Suo, Z. Stretchable Interconnects for Elastic Electronic Surfaces. *Proc. IEEE* **2005**, *93*, 1459–1467.
3. Kim, D.-H.; Lu, N.; Ma, R.; Kim, Y.-S.; Kim, R.-H.; Wang, S.; Wu, J.; Won, S. M.; Tao, H.; Islam, A.; *et al.* Epidermal Electronics. *Science* **2011**, *333*, 838–843.
4. Mannsfeld, S. C. B.; Tee, B. C. K.; Stoltenberg, R. M.; Chen, C. V. H. H.; Barman, S.; Muir, B. V. O.; Sokolov, A. N.; Reese, C.; Bao, Z. Highly Sensitive Flexible Pressure Sensors with Microstructured Rubber Dielectric Layers. *Nat. Mater.* **2010**, *9*, 859–864.
5. Someya, T.; Sekitani, T.; Iba, S.; Kato, Y.; Kawaguchi, H.; Sakurai, T. A Large-Area Flexible Pressure Sensor Matrix with Organic Field-Effect Transistors for Artificial Skin Applications. *Proc. Natl. Acad. Sci. U.S.A.* **2004**, *101*, 9966–9970.
6. Rosset, S.; Niklaus, M.; Dubois, P.; Shea, H. R. Large-Stroke Dielectric Elastomer Actuators with Ion-Implanted Electrodes. *J. Microelectromech. Syst.* **2009**, *18*, 1300–1308.
7. Sekitani, T.; Yokota, T.; Zschieschang, U.; Klauk, H.; Bauer, S.; Takeuchi, K.; Takamiya, M.; Sakurai, T.; Someya, T. Organic Nonvolatile Memory Transistors for Flexible Sensor Arrays. *Science* **2009**, *326*, 1516–1519.
8. Fan, Z.; Razavi, H.; Do, J.-w.; Moriwaki, A.; Ergen, O.; Chueh, Y.-L.; Leu, P. W.; Ho, J. C.; Takahashi, T.; Reichertz, L. A.; *et al.* Three-Dimensional Nanopillar-Array Photovoltaics on Low-Cost and Flexible Substrates. *Nat. Mater.* **2009**, *8*, 648–653.
9. Kraus, T.; Malaquin, L.; Schmid, H.; Riess, W.; Spencer, N. D.; Wolf, H. Nanoparticle Printing with Single-Particle Resolution. *Nat. Nanotechnol.* **2007**, *2*, 570–576.
10. Fan, Z.; Ho, J. C.; Jacobson, Z. A.; Yerushalmi, R.; Alley, R. L.; Razavi, H.; Javey, A. Wafer-Scale Assembly of Highly Ordered Semiconductor Nanowire Arrays by Contact Printing. *Nano Lett.* **2008**, *8*, 20–25.
11. McAlpine, M. C.; Ahmad, H.; Wang, D. W.; Heath, J. R. Highly Ordered Nanowire Arrays on Plastic Substrates for Ultrasensitive Flexible Chemical Sensors. *Nat. Mater.* **2007**, *6*, 379–384.
12. Cheng, W.; Park, N.; Walter, M. T.; Hartman, M. R.; Luo, D. Nanopatterning Self-Assembled Nanoparticle Superlattices by Moulding Microdroplets. *Nat. Nanotechnol.* **2008**, *3*, 682–690.
13. Hwang, J. K.; Cho, S.; Dang, J. M.; Kwak, E. B.; Song, K.; Moon, J.; Sung, M. M. Direct Nanoprinting by Liquid-Bridge-Mediated Nanotransfer Moulding. *Nat. Nanotechnol.* **2010**, *5*, 742–748.
14. Deshmukh, M. M.; Ralph, D. C.; Thomas, M.; Silcox, J. Nanofabrication Using a Stencil Mask. *Appl. Phys. Lett.* **1999**, *75*, 1631–1633.
15. Villanueva, G.; Vazquez-Mena, O.; van den Boogaart, M. A. F.; Sidler, K.; Pataky, K.; Savu, V.; Brugger, J. Etching of Sub-micrometer Structures through Stencil. *Microelectron. Eng.* **2008**, *85*, 1010–1014.
16. Villanueva, L. G.; Martin-Olmos, C.; Vazquez-Mena, O.; Brugger, J.; Langlet, P.; Bausells, J.; Monserrat, J. Localized

Ion-Implantation through Micro/Nanostencil Masks. *IEEE Trans. Nanotechnol.* **2011**, *10*, 940–946.
17. Vazquez-Mena, O.; Villanueva, G.; van den Boogaart, M. A. F.; Savu, V.; Brugger, J. Reusability of Nanostencils for the Patterning of Aluminum Nanostructures by Selective Wet Etching. *Microelectron. Eng.* **2008**, *85*, 1237–1240.
18. Aksu, S.; Yanik, A. A.; Adato, R.; Artar, A.; Huang, M.; Altug, H. High-Throughput Nanofabrication of Infrared Plasmonic Nanoantenna Arrays for Vibrational Nanospectroscopy. *Nano Lett.* **2010**, *10*, 2511–2518.
19. Tun, T. N.; Lwin, M.; Kim, A. H. H.; Chandrasekhar, A. N.; Joachim, C. Wetting Studies on Au Nanowires Deposited through Nanostencil Masks. *Nanotechnology* **2007**, *18*, 335301.
20. Sidler, K.; Vazquez-Mena, O.; Savu, V.; Villanueva, G.; van den Boogaart, M. A. F.; Brugger, J. Resistivity Measurements of Gold Wires Fabricated by Stencil Lithography on Flexible Polymer Substrates. *Microelectron. Eng.* **2008**, *85*, 1108–1111.
21. Sidler, K.; Cvetkovic, N. V.; Savu, V.; Tsamados, D.; Ionescu, A. M.; Brugger, J. Organic Thin Film Transistors on Flexible Polyimide Substrates Fabricated by Full-Wafer Stencil Lithography. *Sens. Actuators, A* **2010**, *162*, 155–159.
22. Vazquez-Mena, O.; Sannomiya, T.; Villanueva, L. G.; Savu, V.; Sidler, K.; Voros, J.; Brugger, J. Metallic Nanodot Arrays Fabricated by Stencil Lithography on SiO_2 and Polymer Substrates. *EIPBN'2010*, Anchorage, AK, 2010.
23. Aksu, S.; Huang, M.; Artar, A.; Yanik, A. A.; Selvarasah, S.; Dokmeci, M. R.; Altug, H. Flexible Plasmonics on Unconventional and Nonplanar Substrates. *Adv. Mater.* **2011**, *23*, 4422–4430.
24. Vazquez-Mena, O.; Villanueva, L. G.; Savu, V.; Sidler, K.; Langlet, P.; Brugger, J. Analysis of the Blurring in Stencil Lithography. *Nanotechnology* **2009**, *20*, 415303.
25. Vazquez-Mena, O.; Sidler, K.; Savu, V.; Park, C. W.; Villanueva, L. G.; Brugger, J. Reliable and Improved Nanoscale Stencil Lithography by Membrane Stabilization, Blurring, and Clogging Corrections. *IEEE Trans. Nanotechnol.* **2011**, *10*, 352–357.
26. Sidler, K.; Villanueva, L. G.; Vazquez-Mena, O.; Savu, V.; Brugger, J. Compliant Membranes Improve Resolution in Full-Wafer Micro/Nanostencil Lithography. *Nanoscale* **2012**, *4*, 773–778.
27. Vazquez-Mena, O.; Sannomiya, T.; Villanueva, L. G.; Voros, J.; Brugger, J. Metallic Nanodot Arrays by Stencil Lithography for Plasmonic Biosensing Applications. *ACS Nano* **2010**, *5*, 844–853.
28. Drummond, C. J.; Chan, D. Y. C. van der Waals Interaction, Surface Free Energies, and Contact Angles: Dispersive Polymers and Liquids. *Langmuir* **1997**, *13*, 3890–3895.
29. Bohren, C. F.; Huffman, D. R. Surface Modes in Small Particles. In *Absorption and Scattering of Light by Small Particles*; John Wiley and Sons, Inc.: New York, 1998.
30. Lamprecht, B.; Schider, G.; Lechner, R. T.; Ditlbacher, H.; Krenn, J. R.; Leitner, A.; Aussenegg, F. R. Metal Nanoparticle Gratings: Influence of Dipolar Particle Interaction on the Plasmon Resonance. *Phys. Rev. Lett.* **2000**, *84*, 4721–4724.
31. Haynes, C. L.; McFarland, A. D.; Zhao, L.; Van Duyne, R. P.; Schatz, G. C.; Gunnarsson, L.; Prikulis, J.; Kasemo, B.; Käll, M. Nanoparticle Optics: The Importance of Radiative Dipole Coupling in Two-Dimensional Nanoparticle Arrays. *J. Phys. Chem. B* **2003**, *107*, 7337–7342.
32. Danckwerts, M.; Novotny, L. Optical Frequency Mixing at Coupled Gold Nanoparticles. *Phys. Rev. Lett.* **2007**, *98*, 026104.
33. Sannomiya, T.; Sahoo, P., K.; Mahcicek, D., I.; Solak, H., H.; Hafner, C.; Grieshaber, D.; Voros, J. Biosensing by Densely Packed and Optically Coupled Plasmonic Particle Arrays. *Small* **2009**, *5*, 1889–1896.
34. Haes, A. J.; Van Duyne, R. P. A Nanoscale Optical Biosensor: Sensitivity and Selectivity of an Approach Based on the Localized Surface Plasmon Resonance Spectroscopy of Triangular Silver Nanoparticles. *J. Am. Chem. Soc.* **2002**, *124*, 10596–10604.
35. Anker, J. N.; Hall, W. P.; Lyandres, O.; Shah, N. C.; Zhao, J.; Van Duyne, R. P. Biosensing with Plasmonic Nanosensors. *Nat. Mater.* **2008**, *7*, 442–453.
36. Sannomiya, T.; Hafner, C.; Voros, J. *In Situ* Sensing of Single Binding Events by Localized Surface Plasmon Resonance. *Nano Lett.* **2008**, *8*, 3450–3455.
37. Mayadas, A. F.; Shatzkes, M. Electrical-Resistivity Model for Polycrystalline Films: The Case of Arbitrary Reflection at External Surfaces. *Phys. Rev. B* **1970**, *1*, 1382–1389.
38. Durkan, C.; Welland, M. E. Size Effects in the Electrical Resistivity of Polycrystalline Nanowires. *Phys. Rev. B* **2000**, *61*, 14215–14218.
39. Vazquez-Mena, O.; Villanueva, G.; Savu, V.; Sidler, K.; van den Boogaart, M. A. F.; Brugger, J. Metallic Nanowires by Full Wafer Stencil Lithography. *Nano Lett.* **2008**, *8*, 3675–3682.